Modeling the phase behavior of polydisperse rigid rods with attractive interactions with applications to single-walled carbon nanotubes in superacids

Micah J. Green,[1,a)] A. Nicholas G. Parra-Vasquez,[1] Natnael Behabtu,[1] and Matteo Pasquali[1,2,b)]
[1]*Department of Chemical and Biomolecular Engineering, Rice University, 6100 Main Street, MS362 Houston, Texas 77005, USA*
[2]*Department of Chemistry, Rice University, 6100 Main Street, MS362 Houston, Texas 77005, USA*

(Received 2 April 2009; accepted 21 July 2009; published online 24 August 2009)

The phase behavior of rodlike molecules with polydisperse length and solvent-mediated attraction and repulsion is described by an extension of the Onsager theory for rigid rods. A phenomenological square-well potential is used to model these long-range interactions, and the model is used to compute phase separation and length fractionation as a function of well depth and rod concentration. The model closely captures experimental data points for isotropic/liquid crystalline phase coexistence of single-walled carbon nanotubes (SWCNTs) in superacids. The model also predicts that the isotropic-biphasic boundary approaches zero as the acid strength diminishes, with the possibility of coexistence of isotropic and liquid crystalline phases at very low concentrations; this counterintuitive prediction is confirmed experimentally. Experimental deviations from classical theories for rodlike liquid crystals are explained in terms of polydispersity and the balance between short-range repulsion and long-range attractions. The predictions of the model also hold practical importance for applications of SWCNT/superacid solutions, particularly in the processing of fibers and films from liquid crystalline SWCNT/superacid mixtures. © *2009 American Institute of Physics*. [DOI: 10.1063/1.3204024]

I. INTRODUCTION

When suspended in a liquid, rodlike molecules and particles transition from an isotropic disordered state to an aligned liquid crystalline (LC) nematic state at sufficiently high concentration. This classical peculiar behavior has generated numerous theories for predicting the isotropic-nematic transition and the equilibrium properties of the coexisting phases; typically, these theories treat the rodlike molecule or particle as an idealized Brownian rigid rod of high aspect ratio. These theories capture with some success the behavior of classical lyotropic LC materials such as LC polymer solutions and rodlike biological particles in water.[1] However, previous theoretical studies fail to describe dispersions of novel anisotropic nanomaterials such as single-walled carbon nanotubes (SWCNTs). Here we extend the theoretical description of polydisperse Brownian rods to include the competition of short-range repulsion and long-range attraction that is known to yield rich behavior in colloidal phases. We focus on the coexistence between the isotropic and nematic phases.

A. Isotropic-nematic phase separation

In 1949, Onsager[2] developed a statistical mechanical theory for the rod orientation distribution function in order to describe the phase behavior of idealized monodisperse rods interacting via a mean field excluded-volume potential in an athermal solvent. This theory is based on the competition between the orientational entropic contribution to the free energy and the excluded-volume potential. This competition gives rise to the isotropic-nematic phase transition that is a characteristic of many rodlike molecules. As rods crowd beyond a critical concentration, alignment occurs spontaneously because orientational ordering is accompanied by a loss of interaction free energy which offsets the partial gain of free energy due to loss in orientational entropy. The predicted coexistence of an isotropic phase and an aligned phase is observed in experimental systems. Onsager's original formulation was numerically refined by Kayser and Raveche[3] and Lekkerkerker *et al.*[4] Later studies extended Onsager's approach to nonhomogeneous systems in order to resolve the profile of the interface between bulk isotropic and nematic regions[5–7] and finite-sized regions.[8] Onsager's approach was also modified to include attractive interactions via a simple order-parameter-based attractive potential by Khokhlov and Semenov;[9,10] Khokhlov and Semenov used the Parsons scaling approximation to allow Onsager's second virial coefficient truncation to remain valid up to the high concentrations that result from the attractive potential.

The major competing theoretical framework for rigid rod phase behavior is Flory's lattice-based theory,[11] which accounts for excluded-volume interactions via packing effects and allows for attractive interparticle interactions governed by the parameter χ. Flory's predictions for the boundaries of the well-known biphasic chimney for an athermal solvent

a)Present address: Department of Chemical Engineering, Texas Tech University, Lubbock, TX 79409. Electronic mail: mgreen@alum.mit.edu.
b)Electronic mail: mp@rice.edu.

(χ=0) are slightly higher ($7.89d/L$, $11.57d/L$) than the Onsager predictions ($3.29d/L$, $4.19d/L$), where d and L are the rod diameter and length, respectively. As the attractive force increases, the biphasic region broadens and the concentration of the coexisting aligned phase grows dramatically such that the coexistence nematic phase is a solid. (The Onsager-based results of Khokhlov[9,10] show a similar broadening effect.) The lattice-based Flory theory allows for great versatility in describing a variety of systems, including mixtures and various types of molecules. Flory and others used the lattice framework to extend models to semiflexible rods,[12] mixtures of rods and flexible coils,[13] rods connected by flexible linkers,[14] rods with flexible side chains,[15] and most relevant to the present study, polydisperse rods.[16] However, the myriad numerical approximations inherent in Flory's treatment have limited the quantitative applications of the theory to anisotropic nanoparticles,[17] particularly those that interact differently at long and short ranges. Moreover, the "attractive" interactions in Flory's theory simply indicate the enthalpy of mixing. In a poor solvent, the rods tend to "attract" one another simply because of the poor compatibility between rod and solvent. This attraction only acts on molecules immediately bordering the rod in the lattice, i.e., at short ranges.

There have been a number of other efforts to describe attractive interactions between rods. A number of studies have focused on depletion forces caused by nonadsorbing polymers in solution with the rods. Surve *et al.*[18] modeled the effects of adsorption in a Flory-type framework, while Bolhuis *et al.*[19] used particle-based simulations to simulate spherocylinders with depletion forces caused by the addition of nonadsorbing polymer. Borukhov and co-workers[20,21] studied attractive depletion forces caused by cross-linkers in the context of stiff biopolymers in aligned phases.

Particle-based simulations have also been used to simulate the phase behavior of rigid rods, usually described as ellipsoids, but these simulations are typically restricted to finite aspect ratio.[22] The free energy of these systems are computed via Monte Carlo methods. Such simulations have been used to simulate the behavior of short aspect ratio spherocylinders interacting through attractive temperature-dependent square-well potentials.[23,24] Because of the shorter aspect ratio and the importance of temperature, these types of simulations are often applied to alkanes,[25,28] far smaller than LC polymers or nanotubes; these simulations have also detected the existence of a nematic-liquid-vapor triple point for these shorter spherocylinders.[25,27] Particle-based simulations provide a useful means of evaluating approximations in Onsager-type frameworks; for instance, Samborski *et al.*[22] used Monte Carlo simulations as a point of comparison for various techniques of computing higher order virial coefficients for the Onsager theory.

B. Effects of polydispersity

In a system of rods, length polydispersity broadens the biphasic region, and long rods preferentially enter the nematic phase, as intuited by Onsager. Moreover, the coexisting isotropic and nematic concentrations depend strongly on the initial (or "parent") concentration of rods. In a solution of monodisperse rods, these coexistence concentrations are independent of the parent concentration; in a solution of polydisperse rods, the increased degree of freedom in the length-dimension yields much richer phase behavior. Initial studies of polydispersity focused on long/short rod mixtures[4] and thick/thin rod mixtures.[7] Simple bidispersity in length or diameter can have important effects, including the formation of nonmonotonic density profiles at the interface.[7]

Three papers in 2003 rigorously analyzed the effects of polydispersity for continuous distributions of rigid rods. Speranza and Sollich[28,29] computed the coexistence concentrations of a system of Onsager rods with continuous polydispersity in length, and they paid special attention to the effects of the longest rods in the distribution. Wensink and Vroege[30] introduced an approximation for the excluded-volume interaction and systematically computed the biphasic boundaries as a function of the initial concentration and the degree of polydispersity. Notably, they found that as polydispersity increases, the isotropic boundary moves to lower concentrations, and the nematic boundary shifts to dramatically higher ones, broadening the biphasic region. These three studies also identified specific scenarios where a triphasic (isotropic, short rod nematic, and long rod nematic) equilibrium state can occur. Although the numerical analysis in Ref. 30 was limited to two forms of the parent population with varying polydispersity, the theory applies to systems described by any rod length distribution.

These studies of polydisperse rod systems were limited to athermal solvents; here we aim to extend this work to include the effect of long-range attraction combined with short-range repulsion.

C. Experimental motivation

The present study is motivated by recent experimental results on the phase behavior of SWCNTs dispersed in superacids, such as fuming sulfuric acid and chlorosulfonic acid.[17,31–33] Since the observation of Iijima and Ichihashi of SWCNTs in 1993,[34] SWCNTs have attracted great interest because of their unique electronic and mechanical properties;[35] much current research is devoted to the creation of neat SWCNT macroscopic articles with properties comparable to the constituent SWCNTs. However, the production of such macroscopic articles has been hindered by the difficulty of dispersing SWCNTs as individual rods.

The dispersion of SWCNTs is difficult because they tend to bundle tightly due to strong van der Waals attraction to each other. Few solvents disperse pristine SWCNTs as individual rods capable of forming a concentrated LC phase. SWCNTs can form a LC solution in water when wrapped or stabilized by acids containing hydrophobic groups such as DNA or hyaluronic acid[36,37] or when trapped in hydrogels.[38] Superacids, such as fuming sulfuric acid and chlorosulfonic acid, are the only fluids that spontaneously disperse SWCNTs as individual rods in a concentrated LC state.[17,31,33] Superacids protonate the sidewalls of SWCNTs and cause

electrostatic repulsion and debundling.[32] These LC dopes have been used for the production of macroscopic SWCNT articles.[17,39,40]

Surprisingly, in superacids weaker than (roughly) equimolar mixtures of sulfuric and chlorosulfonic acids, LC domains are in equilibrium with a dilute isotropic phase. These LC domains are long, threadlike structures, termed "SWCNT spaghetti," composed by a myriad of aligned SWCNTs spaced by a few SWCNT diameters. The SWCNTs can translate along the axis of the strand but have very limited mobility in the normal direction. This unusual phase behavior cannot be described by the Onsager or Flory theories for monodisperse rods because the SWCNTs are polydisperse and because the theories cannot accurately describe the effects of varying acid strength on the inter-rod interactions. In fact, the broadening of the biphasic chimney occurs on the isotropic side rather than the nematic side, contrary to Flory's predictions.

Modeling the phase behavior of such systems would involve both electrostatic forces due to protonation and inter-SWCNT van der Waals attraction. The balance of electrostatic repulsive interactions and van der Waals attractive interactions for dilute polyelectrolyte colloids has been modeled using the Derjaguin, Landau, Verwey, and Overbeek (DLVO) theory.[41,42] The DLVO approach was generalized for interactions between charged anisotropic macromolecules by Chapot *et al.*[43] The DLVO approach has been applied to a number of experiments on aqueous suspensions of charged rods such as V_2O_5 gels[44] and b-FeOOH.[45] DLVO and similar theories cannot be applied to rods in superacids because the assumption of dilute electrolytes inherent in the DLVO theory is inapplicable.

We postulate that the key physical mechanism controlling the behavior of SWCNTs in acids is the competition between long-range van der Waals attraction, which is weakly dependent on the acid strength, and short-range electrostatic repulsion, which depends strongly on the acid strength—as shown clearly by Raman spectroscopy of SWCNTs in acids. We approximate this competition through a simple inter-rod repulsive-attractive potential, where strength of the attractive well varies with solvent quality. The rods interact through an attractive force that varies inversely with the acid strength; this attractive force mimics van der Waals interactions offset to varying degrees by electrostatic repulsion as a function of protonation.

II. FORMULATION

A. Free energy

Our formulation follows that of Wensink and Vroege[30] and includes an additional potential to capture the effect of attractive interparticle interactions and solvent effects. A solution of thin rigid rodlike molecules of diameter d and polydisperse lengths L is described by a rod distribution function $N(l)$. $N(l)$ refers to the number of rods in the system with relative length l, where l is defined as L/L_0 and L_0 is an arbitrary reference length. For a volume V, $N(l)/V$ is the local number density of rods of length l and $\int N(l)dl$ gives the total number of rods in the system.

The dimensionless Onsager excess free energy f for a volume V is written as

$$f = \frac{bF}{Vk_BT} \sim \int c(l)[\ln c(l) - 1]dl + \int c(l)\omega(l)dl + \int\int c(l)c(l')ll'[\rho(l,l') + \lambda(l,l')]dldl', \quad (1)$$

where the reference volume b is defined as $\pi dL_0^2/4$ and the dimensionless rod distribution function $c(l)$ is defined as $bN(l)/V$. The total rod number concentration is c_0, the zeroth moment of the distribution $c(l)$, where distribution moments are defined as

$$c_k = \int c(l)l^k dl. \quad (2)$$

The overall concentration of the system can also be described by the rod volume fraction $\phi=(d/L_0)c_1$. The rod volume fraction is a more experimentally accessible quantity.

The entropic terms in the free energy description can be described as follows. The first term describes the ideal free energy of the polydisperse system. The second term contains the orientational entropy contribution

$$\omega(l) = \int \psi(l,\mathbf{u})\ln[4\pi\psi(l,\mathbf{u})]d\mathbf{u}, \quad (3)$$

where $\psi(l,\mathbf{u})$ is the normalized angular distribution function for rods with relative length l with orientation described by the unit vector $\mathbf{u}$. This term is minimized by a uniform (isotropic) distribution of rod angles written as $\psi=1/4\pi$. The third term contains the excluded-volume interactions between rods. The average excluded-volume contribution from rods of relative length l and l' is

$$\rho(l,l') = \frac{4}{\pi}\int |\mathbf{u}\times\mathbf{u}'|[\psi(l,\mathbf{u})\psi(l',\mathbf{u}')]d\mathbf{u}'d\mathbf{u}. \quad (4)$$

This term is equal to 1 for an isotropic state and is minimized by an aligned nematic state where the rods' alignment minimizes their excluded-volume interactions. The attractive/repulsive potential $\lambda(l,l')$ models inter-rod attraction and repulsion and is new. The phase behavior of idealized Onsager rods is governed by the balance between $\omega(l)$ and $\rho(l,l')$ as a function of $c(l)$.

We follow Wensink and Vroege in using the uniaxial Gaussian ansatz to approximate the angular distribution function $\psi(l,\mathbf{u})$, written as

$$\psi(l,\mathbf{u}) = \begin{cases} \dfrac{\alpha(l)}{4\pi}\exp\left[-\dfrac{1}{2}\alpha(l)\theta^2\right] & \text{for } 0 \le \theta \le \pi/2 \\ \dfrac{\alpha(l)}{4\pi}\exp\left[-\dfrac{1}{2}\alpha(l)(\pi-\theta)^2\right] & \text{for } \pi/2 \le \theta \le \pi, \end{cases} \quad (5)$$

such that $\psi(l,\mathbf{u})$ is reduced to an unknown in only the l-dimension through the function $\alpha(l)$. The function $\alpha(l)$ is left as an unknown that describes the degree of alignment in a given phase. Because of their higher excluded-volume cost, longer rods tend to be more aligned. Wensink and Vroege

wrote $\omega(l) \sim \ln \alpha(l) - 1$ and then developed an asymptotic expansion of $\rho(l,l')$ for the nematic phase in terms of α as

$$\rho(l,l') \sim \sqrt{\frac{8}{\pi}(\alpha(l)^{-1} + \alpha(l')^{-1})}, \tag{6}$$

where terms involving higher powers of $\alpha(l)^{-1}$ are neglected.

We designate variables as pertaining to the isotropic phase, nematic phase, and parent phase by using the superscripts (I), (N), and (0) for the theoretical description of a parent population $c^{(0)}(l)$ phase separating into $c^{(I)}(l)$ and $c^{(N)}(l)$.

B. Equilibrium conditions

The degree of alignment for any nematic equilibrium state must minimize the free energy. In the present case, the degree of alignment is expressed through the unknown $\alpha(l)$, and the condition is written as

$$\frac{\delta f}{\delta \alpha(l)} = 0 = \frac{c(l)}{\alpha(l)} - \left(\frac{8}{\pi}\right)^{1/2} \frac{lc(l)}{\alpha^2(l)} \int l' c(l')(\alpha(l)^{-1} + \alpha(l')^{-1})^{-1/2} dl' + lc(l) \int l' c(l') \frac{\delta \lambda(l,l')}{\delta \alpha(l)} dl'. \tag{7}$$

The excluded-volume term in Wensink and Vroege's equation (7) is incorrect by a factor of two, while their Eq. (8) is correct. We argue below that the function $\lambda(l,l')$ is a weak function of $\alpha(l)$ for the nematic phase such that the final term may be neglected. For an isotropic-nematic coexistence state to exist at equilibrium, two additional criteria must be satisfied. The two phases must have equal chemical potentials $[\mu(l)/k_BT = \delta f/\delta c(l)]$ as a function of l, yielding the condition

$$\ln c^{(I)}(l) + 2lc_1^{(I)} = \ln c^{(N)}(l) + \ln[\alpha(l)] - 1 + \mu_{\text{ex}}^{(N)}(l), \tag{8}$$

and the excess chemical potential for the nematic phase $\mu_{\text{ex}}^{(N)}(l)$ is defined as

$$\mu_{\text{ex}}^{(N)}(l) = 2l \int l' c^{(N)}(l') \lambda(l,l') dl' + 2l \int c^{(N)}(l') l' \rho(l,l') dl'. \tag{9}$$

This criterion must be fulfilled for all l. The two phases must also have the same osmotic pressure $[\Pi = \delta f/\delta V]$ which yields the additional equation

$$c_0^{(I)} + (c_1^{(I)})^2 = c_0^{(N)} + \int lc^{(N)}(l) l' c^{(N)}(l') \times [\rho(l,l') + \lambda(l,l')] dl dl'. \tag{10}$$

Finally, conservation of mass must hold such that the two daughter phases in coexistence must add together to the parent population, i.e.,

$$c^{(0)}(l) = (1-\gamma)c^{(I)}(l) + \gamma c^{(N)}(l), \tag{11}$$

where γ is the volumetric fraction of the system that is nematic. Given a starting population $c^{(0)}(l)$ and attractive potential $\lambda(l,l')$, Eqs. (7), (8), (10), and (11) comprise of three functional equations and one scalar equation that may be solved for $c^{(I)}(l)$, $c^{(N)}(l)$, $\alpha(l)$, and γ. [Alternatively, the normalized parent population $c^{(0)}(l)/c_0^{(0)}$ and γ may be specified with the quantity $c_0^{(0)}$ as an unknown.] For convenience, we take the constant reference length L_0 to be L_{mean}, the average length of the parent population.

The Parsons scaling approach allows for use of the Onsager excluded volume at high concentrations.[10] The difference in excluded volume is less than 5% for $\phi < 0.2$. We adapt the Parsons scaling approach for polydisperse systems to write the excluded-volume term of the free energy as

$$\frac{bF_{\text{Parsons}}}{Vk_BT} \sim \int c(l) \left(\frac{L_0}{d}\right) l(-\ln(1-\phi(l'))) \rho(l,l') dl dl'. \tag{12}$$

After some mathematical manipulation, the contributions to the chemical potential and osmotic pressure are then written as

$$\Pi_{\text{Parsons}} \sim \int \frac{c(l)c(l')ll'\rho(l,l')}{(1-\phi(l'))} dl dl', \tag{13}$$

$$\mu_{\text{Parsons}} \sim \left(\frac{L_0}{d}\right) l \int (-\ln(1-\phi(l))) \rho(l,l') dl' + \frac{l}{(1-\phi(l'))} \int c(l') l' \rho(l,l') dl'. \tag{14}$$

The equation for equilibrium alignment becomes

$$\frac{\delta f}{\delta \alpha(l)} = 0 = \frac{2c(l)}{\alpha(l)} - \left(\frac{8}{\pi}\right)^{1/2} \left(\frac{L_0}{d}\right) \frac{lc(l)}{2\alpha^2(l)} \int (-\ln(1-\phi(l'))) \times \left[(\alpha(l)^{-1} + \alpha(l')^{-1})^{-1/2} + \frac{\delta \lambda(l,l')}{\delta \alpha(l)} \right] dl' - \left(\frac{8}{\pi}\right)^{1/2} \left(\frac{L_0}{d}\right) \frac{(-\ln(1-\phi(l)))}{2\alpha^2(l)} \int l' c(l') \times \left[(\alpha(l)^{-1} + \alpha(l')^{-1})^{-1/2} + \frac{\delta \lambda(l,l')}{\delta \alpha(l)} \right] dl', \tag{15}$$

C. Attractive and repulsive interactions

The novel contribution to the free energy expression is expressed in the quantity $\lambda(l,l')$. We propose a particular phenomenological model inspired by the unusual SWCNT spaghetti LC phase illustrated in Fig. 1; the SWCNTs in these strands are aligned along the strand with small distances between SWCNT sidewalls. The SWCNTs are no longer in align due to the short-range electrostatic repulsion, but the attractive forces keep them within a few diameters of each another, such that each SWCNT interacts with an effective "cage" of other SWCNTs within the LC phase.

Our proposed model is as follows. A rod in an aligned state is subject to an attractive interaction with surrounding rods $u(D)$, which represents the energy per unit length of the rod as a function of the distance D between the centers of the aligned rods. This quantity scales linearly with l and is made dimensionless as $U(D) \equiv u(D)L_{\text{mean}}/k_BT$. The square-well

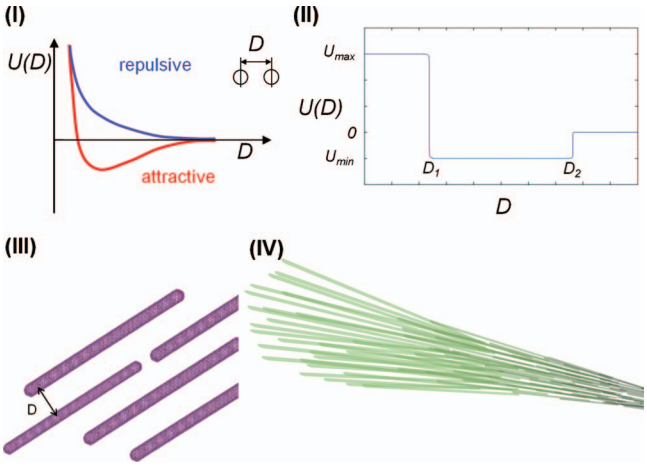

FIG. 1. (i) The combination of short-range electrostatic repulsive forces (shown in blue) and van der Waals attraction will result in an attractive well (shown in red) potential between the two particles. However, the exact form of these functions is unknown for complex solvent and solutes such as superacids and SWCNTs. (ii) A simple phenomenological square well potential $U(D)$ is used to capture this balance of repulsive forces and attractive forces between SWCNTs in various acids. As the acid quality decreases, the well becomes deeper. (iii) D is the distance between neighboring SWCNTs in the LC phase. This simplified potential is inspired by the unusual LC order seen in "spaghetti" in SWCNT/superacid systems (Ref. 33). (Iv) A schematic of spaghetti geometry depicts the threadlike, aligned nature of these unusual LC domains.

potential $U(D)$ is depicted in Fig. 1 and is characterized by the four parameters: $U_{\max}$, $U_{\min}$, D_1, and D_2. The discontinuities in the derivatives of the square-well potential are made continuous by using an arctan function to approximate the transitions of $U(D)$ across D_1 and D_2.

As a first approximation, this attractive interaction is applied only to the dense nematic phase. This is motivated by experimental observations of the unusual LC phases in SWCNT/superacid systems. The LC phase is marked by aligned SWCNTs in long threadlike domains with acid molecules in between, and the inter-SWCNT distances are of the order of 10–30 nm. This means that rods in the nematic phase are separated by average distances that are much smaller than the average distances between rods in the isotropic phase. This means that the rods in the nematic phase will spend substantially more time in the attractive well than rods in the isotropic phase; we approximate these experimental observations simply by applying the attractive well to the nematic phase but not the isotropic phase. The attractive interaction varies weakly with alignment in nematic phases. On average, the nematic phase will behave much like a columnar phase where the average inter-rod distance D can be calculated from $\phi^{(N)}$, the rod volume fraction in the nematic phase, as

$$D = \frac{d}{2}\left(\frac{\phi^{(N)}\sqrt{3}}{2\pi}\right)^{-1/2}. \tag{16}$$

As the "test" rod feels the attractive potential, the rod's nearest neighbors in the densely packed nematic phase will "shield" the rod from others that are farther out such that the attractive interaction is minimal beyond those nearest neighbors. (Also, those nearest neighbors will be the first to enter the repulsive region.) Consequently, the quantity $lc(l)\int l' c(l')\lambda(l,l')dl'$ is rewritten as $lc(l)\Lambda(l)$, where $\Lambda(l) = 6U(D)$. (A similar argument is used by Wensink and Vroege in the case of average excluded volume in the nematic phase.) The square-well potential can be parametrized by the dimensionless quantities $U_{\max}$, $U_{\min}$, D_1/d, and D_2/d, which may vary with solvent quality. In addition, the repulsive region ($D < D_1$) increases the effective excluded volume by a factor of $(D_1/d+1)/2$. The repulsive portion of the square-well potential is applied to both isotropic and nematic phases.

D. Shadow and cloud phases

The phase behavior of polydisperse rod populations is complicated by the fact that the parent population $c^{(0)}(l)$ influences the properties of the daughter populations $c^{(I)}(l)$ and $c^{(N)}(l)$. This stands in contrast to the monodisperse case where the coexistence values of $c_0^{(I)}$ and $c_0^{(N)}$ are independent of the parent concentration $c_0^{(0)}$. These concepts are illustrated in Fig. 2, which depicts the dependence of $c_0^{(I)}$ and $c_0^{(N)}$ on $c_0^{(0)}$. A thorough explanation of cloud and shadow phases may be found in the Appendix.

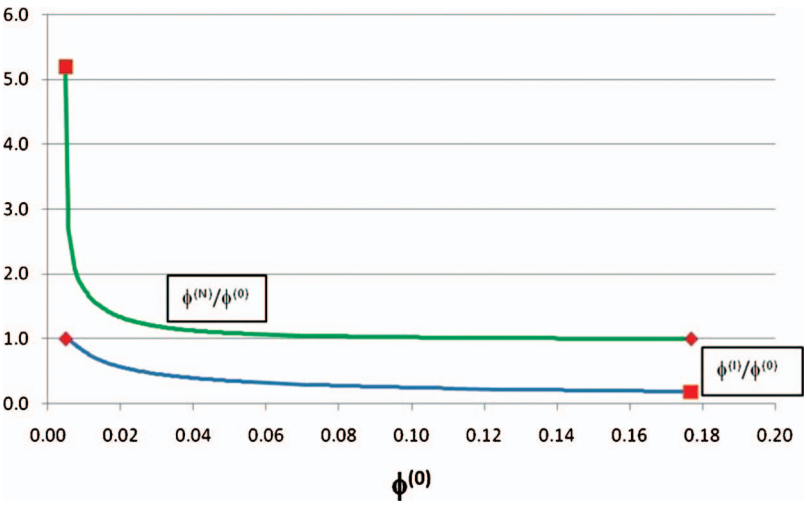

FIG. 2. Computational results for an athermal solvent illustrating the dependence of $\phi^{(I)}$ and $\phi^{(N)}$ on $\phi^{(0)}$ for polydisperse distributions for or $\sigma=0.6$ and $L_{\text{mean}} = 348d$. Squares indicate shadow points, and diamonds indicate cloud points. This stands in Stark contrast to the monodisperse case where $\phi^{(I)}$ and $\phi^{(N)}$ do not vary.

E. Parent distribution and solution method

For the SWCNT samples of interest, the parent rod population is well described by a simple Schultz distribution

$$c^{(0)}(l)/c_0^{(0)} = Nl^z \exp[-(z+1)l], \tag{17}$$

with normalization factor N and is truncated at some minimum and maximum l. The polydispersity of any population is described by the parameter σ, defined as

$$\sigma^2 = c_2^{(0)}/(c_1^{(0)})^2 - 1, \tag{18}$$

which is related to the parameter z in the Schultz distribution as $\sigma^2=(1+z)^{-1}$.

In a typical purified batch of HiPco SWCNTs (HPR batch 152.2), we find that the parent distribution of SWCNTs is well approximated through the Schultz distribution as follows: $d=1$ nm, $L_{mean}=348$ nm, $L_{min}=17$ nm (the SWCNT purification process eliminates SWCNTs below a particular cutoff), $L_{max}=8$ μm, and $\sigma=0.6$.[46] We use this as an example parent population.

In general, we explore numerically the phase behavior of a SWCNT dispersion as a function of the attractive potential well depth U_{min}, concentration ϕ_0, and of the polydispersity σ. For all studies, we set $U_{max} \gg |U_{min}|$ since variations in U_{max} do not substantially change the phase behavior as long as $U_{max}>1$, and we set $D_2/d \gg 1$ because nematic phases where $D>D_2$ do not differ from the athermal case.

The l-space is discretized into Q points in a fashion similar to that described by Wensink and Vroege, and Eqs. (7), (8), (10), and (11) are discretized into $3Q+1$ nonlinear equations and solved simultaneously using Newton's method. Solutions are traced in $c_0^{(0)}$-space (or γ-space), σ-space, and U_{min}-space using arc length continuation in the parameter of interest.[19] The following results and discussion are specific to the Schultz distribution but should be representative of the behavior of other parent populations. (A typical value for Q is 70. Note that the points need not be evenly spaced.)

III. RESULTS AND DISCUSSION

A. Cloud curves

For the example population of rods described above with $\sigma=0.6$, the isotropic and nematic cloud curves are computed as a function of U_{min} for the case where $D_1/d=1$ (Fig. 3). $U_{min}=0$ corresponds to polydisperse athermal rods, the isotropic cloud point is $\phi^{(I)}=0.0049$, and the nematic cloud point is $\phi^{(N)}=0.177$.

As attractive interactions grow, the nematic phase becomes more thermodynamically favorable and more concentrated. Because $D_1/d=1$, the aligned rods can pack tightly together in the LC phase so the nematic cloud curve moves rapidly to the maximum packing fraction as U_{min} decreases. Setting $D_1/d>1$ essentially sets a minimum for inter-rod spacing and a maximum $\phi^{(N)}$. Such a case is shown as a dotted line in Fig. 3 for $D_1/d=2.08$, where the increase in $\phi^{(N)}$ is arrested by short-range repulsion.

The nematic cloud curve in Fig. 3 for $D_1/d=1$ is similar to the classic Flory theory[11] and the Khokhlov extension of the Onsager theory[9] because the biphasic region primarily

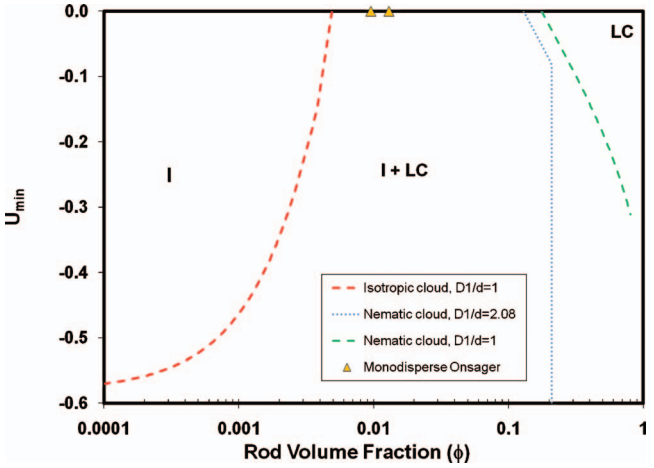

FIG. 3. The isotropic and nematic cloud points are depicted as a function of the well depth U_{min} for $\sigma=0.6$ and $L_{mean}=348d$. When $D_1/d=1$, the nematic cloud point rapidly increases to $\phi^{(N)}=1$ as U_{min} decreases. For the case $D_1/d=2.08$, $\phi^{(N)}$ remains constant at 0.210. The Onsager predictions for monodisperse rods are depicted as triangles (△).

broadens by increasing the concentration of the nematic cloud curve $\phi^{(N)}$ toward the maximum packing fraction (0.907) as the solvent quality decreases. In all these previous studies, the nematic concentration rapidly increases to a solidlike state because short-range repulsion is not included in the model. The Parsons scaling approach causes the cloud curve to level off, similar to the results of Khokhlov *et al.*

Most interestingly, the isotropic cloud curve diverges to very small values at a critical value of $U_{min}^* \cong -0.581$. Because $\log c^{(I)}(l) \sim l\phi^{(N)}U_{min}$, the quantity $\log \phi^{(I)}$ will become more and more negative as the attractive force in the nematic phase increases. Therefore in systems where attractive interactions are stronger than this critical value, the dilute, isotropic phase must always coexist with some LC phase. Even at very small concentrations, the system is still in the biphasic regime; thus, some rods will form an aligned phase at equilibrium due to the strong attraction. A similar result was found by Speranza and Sollich; for distributions with small amounts of extremely long rods, the cloud curve decreased to vanishingly small concentrations.[28] This holds great importance for experimental studies of rod dispersions, as discussed below. Figures 4 and 5 show the influence of polydispersity σ on the isotropic and nematic cloud curves for $D_1/d=1$.

As polydispersity decreases, the isotropic cloud curves move down to lower well depths and to the right to higher rod concentration; this is to be expected since the effects of length fractionation decrease as polydispersity decreases. This also means that U_{min}^* decreases as a function of σ; this holds practical importance for experimental scenarios where an isotropic solution is desired. If a particular solvent/rod combination corresponds to a value of U_{min} that is less than U_{min}^*, then even dilute solutions will be in the biphasic regime. If the polydispersity of the solution can be decreased and/or the average length increased, then the value of U_{min}^* will also decrease; thus, polydispersity can be used as a control to ensure that $U_{min}>U_{min}^*$.

As polydispersity decreases, the nematic cloud curve

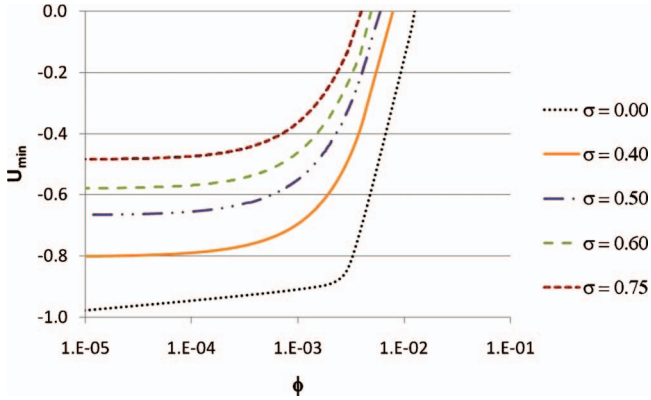

FIG. 4. Isotropic cloud curves (U_{min} vs ϕ) as a function of σ for $D_1/d=1$. As σ decreases, the isotropic cloud curves move down to lower well depths and to the right to higher rod concentration as length fractionation effects diminish. The critical value of U^*_{min} drops with decreasing σ.

moves down to lower well depths and to the left to lower rod's concentration. For low σ, the nematic cloud curve is a much weaker function of acid strength than the isotropic cloud curve. Thus, for broad distributions (e.g., $\sigma=0.6$), the nematic cloud curve varies more rapidly than the isotropic cloud curve, while for narrow distributions (e.g., $\sigma=0.4$), the opposite is true. Note that in the monodisperse case, the nematic cloud curve actually decreases with the attractive well becomes stronger; this differs from the polydisperse case because the attractive well amplifies the effects of polydispersity and broadens the biphasic region.

B. Comparison with experiment

In previous papers, we used a series of experiments to establish a phase diagram for SWCNT/acid mixtures[17,31] which is displayed in Fig. 6. Various SWCNT/acid mixtures at a given SWCNT concentration (denoted by diamonds in Fig. 6) are centrifuged into isotropic and nematic phases, and the concentration $\phi^{(I)}$ of the isotropic phase is measured using UV-vis-near infrared (NIR) absorbance and marked as black circles. The concentration $\phi^{(I)}$ grows with increasing fractional charge (better solvent quality). In contrast to the predictions of Flory-type theories, the dilute isotropic phase

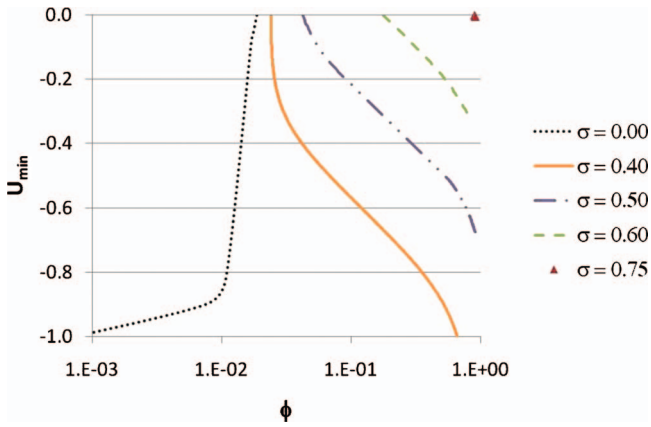

FIG. 5. Nematic cloud curve for $D_1/d=1$ for various values of σ. The cloud curves increase to $\phi=1$ as attractive interactions increase, but this effect diminishes with decreasing σ.

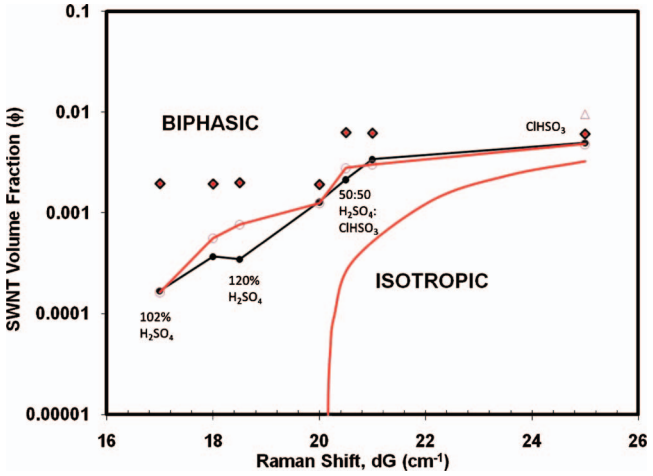

FIG. 6. SWCNT/superacid phase behavior as a function of SWCNT volume fraction and acid strength (measured by dG). Black symbols denote experimental results (Ref. 17) Red symbols refer to theoretical predictions, and red open circles (○) designate the theoretical predictions for $\phi^{(I)}$ compared with experimental measurements of $\phi^{(I)}$, denoted by black circles (●). Black/red diamonds (◇) indicate the initial system concentration $\phi^{(0)}$ for both experiments and simulations of isotropic (i)—LC phase separation. The open red triangles (△) is the Onsager predictions for $\phi^{(I)}$ for a system of monodisperse hard rods. Red line (–) represents the theoretical predictions for the isotropic cloud curve. Simulations are for $\sigma=0.6$, $L_{mean}=348d$, and $D_1/d=2.08$.

in poor solvents coexists with a concentrated LC phase ($\phi^{(N)}\approx 0.1$) rather than with a solid phase (i.e., $\phi^{(N)}>0.9$).

In order to compare the theoretical results with the experimental results for SWCNTs in superacids, a relationship between U_{min} and acid strength must be posited. Superacid strength is typically measured in terms of base-specific Hammett acidity.[47] In the case of SWCNT/superacid systems, acid strength is related to the fractional charge per carbon caused by protonation of the nanotube sidewall.[31] (This quantity varies linearly with the wavenumber shift, dG, of the G-peak in the SWCNT Raman spectra.) The van der Waals forces should be roughly independent of the acid strength. However, as the degree of protonation increases, the repulsion effect increases. Thus, U_{min}, which represents the sum of the van der Waals forces and the repulsive forces, becomes shallower as the acid strength increases.[48] We approximate the dependence of the repulsive force on the acid strength by positing a simple linear relationship between dG and the attractive well depth U_{min} by comparing the theoretical and experimental results for the isotropic concentration after phase separation.[49]

Experimental measurements for the strongest acid used (chlorosulfonic acid) indicate that $\phi^{(I)}$ is approximately equal to the theoretical predictions for athermal (Onsager) rods; thus, we match a Raman shift of $dG=25$ cm^{-1} to $U_{min}=0$. The theoretical predictions for $\phi^{(I)}$ for $U_{min}=-0.957$ match the values of $\phi^{(I)}$ from centrifugation experiments on SWCNTs in 102% H_2SO_4 (i.e., 100% H_2SO_4 with excess 2 wt % dissolved SO_3) which has a Raman shift of $dG=17$ cm^{-1}. These two data points set the linear relationship between U_{min} and dG.

Figure 6 combines the computational and experimental results in a full phase diagram for SWCNT/acid mixtures.

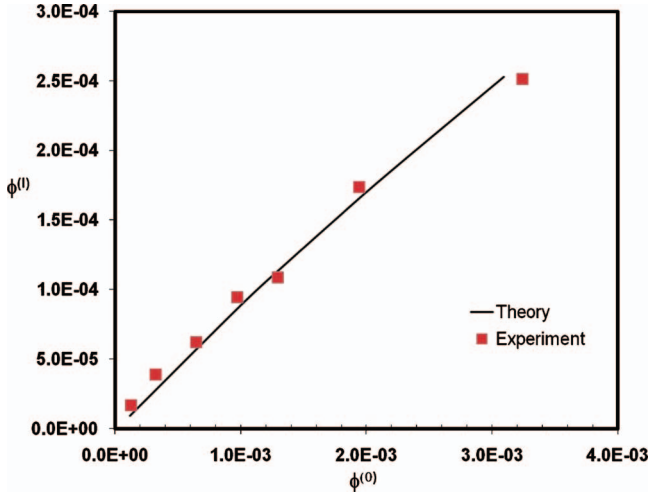

FIG. 7. SWCNT/120 H_2SO_4 mixtures of varying $\phi^{(0)}$ were prepared and phase separated; the isotropic concentration $\phi^{(0)}$ was measured by UV-vis-NIR absorbance. These experimental measurements showed a close match with theoretical predictions (σ=0.6 and L_{mean}=348d) for phase separation as a function of $\phi^{(0)}$.

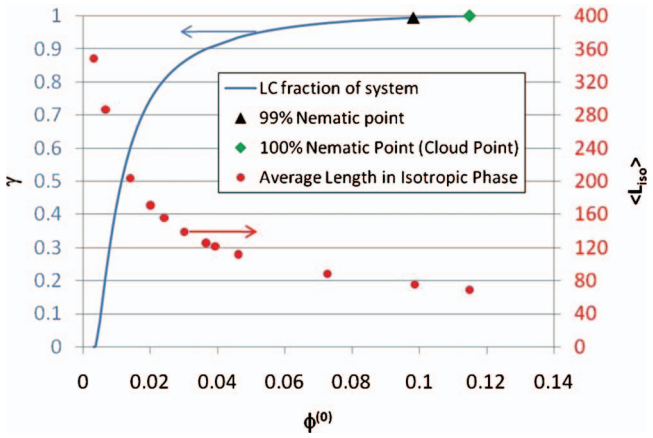

FIG. 8. (Left) Volumetric fraction of system that is nematic (denoted as γ) as a function of $\phi^{(0)}$ for for U_{min}=0, σ=0.6, L_{mean}=348d, and D_1/d=2.08. The system reaches γ=0.95 at $\phi^{(0)} \approx 0.1$ (noted as triangle), but the concentration must increase to $\phi^{(0)}$=0.115 in order to reach γ=1 (the nematic cloud point, noted as diamond). Experimental data indicate a cloud point of $\phi^{(0)} \approx 0.1$ but cannot detect the small isotropic regions filled with short rods that persist up to $\phi^{(0)}$=0.115. (Right) Average length of rods in the isotropic phase (denoted as $\langle L_I \rangle$) as a function of $\phi^{(0)}$. Near the isotropic cloud point, $\langle L_I \rangle$ approaches that of the parent population, but $\langle L_I \rangle$ decreases dramatically as $\phi^{(0)}$ approaches the nematic cloud point. Thus, near the nematic cloud point, the rods in the isotropic phase tend to be the shortest rods in the parent distribution, as confirmed experimentally elsewhere (Ref. 50).

The model (red open circles) is remarkably successful at predicting the experimental values $\phi^{(I)}$ (black circles) at low concentrations.[17] Therefore, the simple square-well potential captures the chief aspects of the physical interactions between SWCNTs in acids.

Additional experiments were performed using the methods of Rai *et al.*[31] to test the model. The concentration $\phi^{(I)}$ of the isotropic phase in 120% H_2SO_4 was measured as a function of the starting concentration $\phi^{(0)}$. A comparison between theoretical and experimental data points is displayed in Fig. 7. Again, the agreement between the two shows that the fundamental physics of internanotube interactions are captured by the theory.

Experimental measurements indicate a nematic cloud point of $\phi^{(N)} \approx 0.1$ that is relatively constant with respect to the acid strength; however, the theoretical results indicate a slightly constant value of $\phi^{(N)}$=0.115. Unlike the case of low-concentration phase separation, the theoretical and experimental values for the nematic cloud curve do not match. However, further analysis of the theoretical results reveals why the values differ. In Fig. 8, the theory predicts that $\gamma \approx 0.99$ for a system where $\phi^{(0)}$=0.1, i.e., 99% of the system (by volume) is nematic. The remaining 1% is isotropic and comprised of relatively short rods, as shown in Fig. 8. In an experiment, these short-rod-dominated isotropic regions would be found primarily in the defects between LC domains, and these small isotropic regions would be nearly undetectable by optical microscopy, rheology, or dynamic scanning calorimetry. Thus, the experimental points are best taken as measurements of the transition to a system that is 99% LC by volume, and we may take the theoretical prediction of the nematic cloud point as correct. The theory predicts that the starting concentration must be pushed up to $\phi^{(0)}$=0.115 to completely eliminate these isotropic regions. However, simulation results also indicate that if all of the rods with an aspect ratio under 40 are removed, then the nematic cloud curve decreases below $\phi^{(0)} \approx 0.1$.

This system does not appear to show signs of nematic-nematic (N-N) coexistence. Such coexistence has been shown in prior studies in two contexts: (1) Wensink and Vroege[30] predicted that for a limited σ and $\phi^{(0)}$ range, two nematic phases coexist, one predominantly composed of short rods and the other composed of long rods. Although entropic considerations favor no difference in length distribution between the two phases, this length fractionation is caused by free energy penalties on differences in alignment. For HiPco SWCNT systems, the experimentally relevant σ and $\phi^{(0)}$ values lie outside the range for N-N coexistence. (2) Monodisperse square-well spherocylinder studies of Varga *et al.*,[51] among others, indicate the presence of a narrow region in U_{min}-space where a low-concentration nematic phase is in coexistence with a high-concentration nematic phase to the right of the biphasic (isotropic-nematic) chimney. This is similar to the findings of Flory and others.[11,15] The presence of such a region can be detected by a turning point in phase space for the nematic solution; for our system, no such turning point was detected for the monodisperse case.

C. Applications

The computational results show that a LC phase will always be present for acids with $dG < 20.15$ cm^{-1} ($U_{min} < U^*_{min}$, where U^*_{min}=−0.581, equivalent to an acid mixture with a 9:16 volume ratio of $ClSO_3H$ to H_2SO_4), regardless of the starting SWCNT concentration. This means that in order to get a dilute isotropic suspension of individual SWCNTs in superacid, the solution must first be centrifuged and phase separated in order to remove the isotropic phase from the nematic phase. A number of CNT characterization techniques (such as rheological characterization of CNT length[52]) re-

quire a dilute, isotropic suspension, and these counterintuitive computational results show that a simple low-concentration dispersion of SWCNTs in 120% H_2SO_4 will not yield a dilute isotropic solution. The isotropic cloud curve can be moved down to lower well depths and to the right to higher rod concentrations by eliminating the longest SWCNTs in a given sample; this would be useful for applications requiring a dilute isotropic solution and could be accomplished via a number of experimental techniques.

Also, one of the chief applications of SWCNT/superacid dispersions is the formation of aligned articles such as fibers and films;[17,39] our computational results have immediate applications for the processing of such articles. The fiber spinning process works as follows high-concentration LC SWCNT/superacid dispersions are mixed and extruded. The viscous dispersion becomes more aligned due to the tension on the fluid during extensional flow. Finally, the dispersion is coagulated in a nonsolvent bath where the acid is removed, and the SWCNT dispersion solidifies to form an aligned fiber. The best fibers are produced by dispersions that are highly aligned and fully liquid crystalline, i.e., above the nematic cloud curve. Any isotropic regions in the dispersions form misaligned, weak regions in the final fiber; these defects decrease the electrical properties and are the primary points of fiber mechanical failure. [Note that defects that are predominantly composed of small nanotubes have already been observed for LC multiwalled CNT (MWCNT) systems.[50]]

With this application in mind, the theoretical framework outlined above can be used to locate the true nematic cloud curve in order to ensure that the dispersion is fully LC. In this case, the cloud curve concentration may be too high for practical mixing and fiber spinning so the theoretical framework can also be used to test the results of manipulating the starting SWCNT length distribution in order to decrease the nematic cloud concentration. In this case, the elimination of SWCNTs under 40 nm will decrease the nematic cloud concentration below $\phi^{(0)} \approx 0.1$ such that SWCNT/superacid dopes of $\phi^{(0)} \approx 0.1$ will be fully LC.[53]

Also, this theoretical framework has implications for high-concentration rheology of SWCNT dispersions. The dependence of viscosity on concentration is a well-known experimental test for liquid crystallinity; the viscosity increases, goes through a maximum, decreases due to the formation of a LC phase, and finally begins to increase again at high concentrations.[33] This dependence on concentration is blurred and weakened as the biphasic chimney is broadened because the formation of aligned phase occurs over a much wider concentration range. SWCNT/superacid dispersions with weaker acids or polydisperse length distributions will show a weak dependence of viscosity on concentration and may not show the maximum/minimum signature of liquid crystallinity. Decreasing polydispersity or strengthening the acid solvent will sharpen and amplify the difference between the maximum and minimum in viscosity.

The utility of the theoretical treatment outlined in this study is evident from the unexpected nature of the results. Optical microscopy experiments and differential scanning calorimetry (DSC) could not detect the isotropic regions in the SWCNT/superacid dispersions used for fiber spinning at $\phi^{(0)} \approx 0.1$, but the theory predicts that these regions are indeed present; such regions have adverse effects on as-spun fibers. Also, it is entirely intuitive to reason that a dilute solution of SWCNTs in 120% H_2SO_4 would be dispersed as isotropic individuals, but the theory predicts that even these low concentrations are within the biphasic region because of attractive interactions.

We expect that this analysis will pave the way for the modeling of other anisotropic materials such as (MWCNTs) or inorganic nanorods. The phase behavior of CdSe nanorods[54] has been assessed through purely qualitative means, and an effective theoretical framework for understanding these materials is needed. The phase transitions for solutions of polydisperse functionalized MWCNTs were qualitatively characterized by Song and co-workers.[55,56] A theoretical analysis of these systems may allow a more quantitative understanding of these dispersed nanomaterials.

D. Conclusions

We have developed an extension to the Onsager theory for polydisperse rigid rods developed by Wensink and Vroege in order to capture the balance of long-range attractive and repulsive forces observed for anisotropic nanomaterials in solution. Our work is particularly motivated by the recent quantitative experimental data for SWCNTs dispersed as individual rigid rods in superacids. Our results indicate excellent agreement between the theoretical and the experimental data for predicting phase separation at low concentrations and for predicting the biphasic chimney's broadening on the isotropic side. The theoretical results also hold important and surprising implications for a variety of SWCNT/superacid experiments and applications, including the understanding of SWCNT/superacid rheology and the processing of fibers and films from LC dopes.

ACKNOWLEDGMENTS

We acknowledge the help of Virginia Davis, Pradeep Rai, Valentin Prieto, Howard Schmidt, Robert Hauge, Rick Smalley, and Wade Adams. Funding was provided by the Office of Naval Research under Grant No. N00014-01-1-0789, AFOSR Grant No. FA9550-06-1-0207, AFRL Agreement Nos. FA8650-07-2-5061 and 07-S568-0042-01-C1, NSF CAREER, and the Evans-Attwell Welch Postdoctoral Fellowship. This material was based on research sponsored by Air Force Research Laboratory under Agreement No. FA8650-07-2-5061.

APPENDIX: CLOUD AND SHADOW PHASES

Two useful but often-misunderstood concepts for delineating the phase behavior of polydisperse rod populations are the cloud phase and shadow phase. For example, at small concentrations, a parent population of polydisperse rods in an athermal solvent will remain isotropic with no phase separation. As the parent concentration $c_0^{(0)}$ is increased, a point is reached where an infinitesimal volume of nematic phase, termed a "shadow phase," forms, while the vast majority of the parent population remains in the "cloud" isotropic phase.

Thus, the shadow nematic phase coexists with the cloud isotropic phase, and the corresponding value of $c_0^{(0)}$ represents the lowest value of $c_0^{(0)}$ at which coexistence is possible. The converse is true on the high-concentration side of the phase diagram; the shadow isotropic phase coexists with the cloud nematic phase, and the corresponding value of $c_0^{(0)}$ represents the highest value of $c_0^{(0)}$ at which coexistence is possible. On the isotropic cloud curve, the quantity γ (the fraction of the system that is nematic) will approach 0, while on the nematic cloud curve, γ will approach 1.

The isotropic and nematic cloud phases are the ultimate boundaries of the biphasic region in a system of polydisperse rods. Parent populations within the biphasic region will phase separate into coexisting isotropic and nematic phases, and the values of $c_0^{(I)}$ and $c_0^{(N)}$ will vary with $c_0^{(0)}$. These concepts are illustrated in Fig. 2, which depicts the dependence of $c_0^{(I)}$ and $c_0^{(N)}$ on $c_0^{(0)}$. Note that the daughter phases appear to remain in the biphasic regime which suggests that they are not an equilibrium solution; this paradox is resolved by the fact that the daughters have a different length distribution than the parent phase, such that the daughter phases lie outside the cloud curves for their specific distribution.

[1] Z. Dogic, K. R. Purdy, E. Grelet, M. Adams, and S. Fraden, Phys. Rev. E **69**, 051702 (2004).
[2] L. Onsager, Ann. N.Y. Acad. Sci. **51**, 627 (1949).
[3] R. F. Kayser and H. J. Raveche, Phys. Rev. A **17**, 2067 (1978).
[4] H. N. W. Lekkerkerker, P. Coulon, R. Van Der Haegen, and R. Deblieck, J. Chem. Phys. **80**, 3427 (1984).
[5] Z. Y. Chen and J. Noolandi, Phys. Rev. A **45**, 2389 (1992).
[6] D. L. Koch and O. G. Harlen, Macromolecules **32**, 219 (1999).
[7] K. Shundyak and R. van Roij, J. Phys.: Condens. Matter **13**, 4789 (2001).
[8] M. J. Green, R. C. Armstrong, and R. A. Brown, J. Chem. Phys. **125**, 214906 (2006).
[9] A. R. Khokhlov, in *Liquid Crystallinity in Polymers*, edited by A. Ciferri (VCH, New York, 1991).
[10] A. R. Khokhlov and A. N. Semenov, J. Stat. Phys. **38**, 161 (1985).
[11] P. J. Flory, Proc. R. Soc. London, Ser. A **234**, 73 (1956).
[12] P. J. Flory, Proc. R. Soc. London, Ser. A **234**, 60 (1956).
[13] P. J. Flory, Macromolecules **11**, 1138 (1978).
[14] P. J. Flory, Macromolecules **11**, 1141 (1978).
[15] M. Ballauff, Macromolecules **19**, 131 (1995).
[16] P. J. Flory and A. Abe, Macromolecules **11**, 1119 (1978).
[17] V. A. Davis, A. N. G. Parra-Vasquez, M. J. Green, P. K. Rai, N. Behabtu, V. Prieto, R. D. Booker, J. Schmidt, E. Kesselman, W. Zhou, H. Fan, W. W. Adams, R. H. Hauge, J. E. Fischer, Y. Cohen, Y. Talmon, R. Smalley, and M. Pasquali, "True solutions single walled carbon nanotubes for assembly into macroscopic materials," Nature Nanotechnology (in press).
[18] M. Surve, V. Pryamitsin, and V. Ganesan, Macromolecules **40**, 344 (2007).
[19] P. G. Bolhuis, A. Stoobants, D. Frenkel, and H. N. W. Lekkerkerker, J. Chem. Phys. **107**, 1551 (1997).
[20] I. Borukhov and R. F. Bruinsma, Phys. Rev. Lett. **87**, 158101 (2001).
[21] I. Borukhov, R. F. Bruinsma, W. M. Gelbart, and A. J. Liu, Proc. Natl. Acad. Sci. U.S.A. **102**, 3673 (2005).
[22] A. Samborski, G. T. Evans, C. P. Mason, and M. P. Allen, Mol. Phys. **81**, 243 (1994).
[23] B. Martinez-Haya, A. Cuetos, and S. Lago, Phys. Rev. E **67**, 051201 (2003).
[24] A. Cuetos, B. Martinez-Haya, L. F. Rull, and S. Lago, J. Chem. Phys. **117**, 2934 (2002).
[25] D. C. Williamson and Y. Guevara, J. Phys. Chem. B **103**, 7522 (1999).
[26] A. Samborski and G. T. Evans, Mol. Phys. **80**, 1257 (1993).
[27] D. C. Williamson and F. del Rio, J. Chem. Phys **109**, 4675 (1998).
[28] A. Speranza and P. Sollich, Phys. Rev. E **67**, 061702 (2003).
[29] A. Speranza and P. Sollich, J. Chem. Phys. **118**, 5213 (2003).
[30] H. H. Wensink and G. J. Vroege, J. Chem. Phys. **119**, 6868 (2003).
[31] P. K. Rai, R. A. Pinnick, A. N. G. Parra-Vasquez, V. A. Davis, H. K. Schmidt, R. H. Hauge, R. E. Smalley, and M. Pasquali, J. Am. Chem. Soc. **128**, 591 (2006).
[32] S. Ramesh, L. M. Ericson, V. A. Davis, R. K. Saini, C. Kittrell, M. Pasquali, W. E. Billups, W. W. Adams, R. H. Hauge, and R. E. Smalley, J. Phys. Chem. B **108**, 8794 (2004).
[33] V. A. Davis, L. M. Ericson, A. N. G. Parra-Vasquez, H. Fan, Y. Wang, V. Prieto, J. A. Longoria, S. Ramesh, R. K. Saini, C. Kittrell, W. E. Billups, W. W. Adams, R. H. Hauge, R. E. Smalley, and M. Pasquali, Macromolecules **37**, 154 (2004).
[34] S. Iijima and T. Ichihashi, Nature (London) **363**, 603 (1993).
[35] R. H. Baughman, Science **290**, 1310 (2000).
[36] S. Badaire, C. Zakri, M. Maugey, A. Derré, J. N. Barisci, G. Wallace, and P. Poulin, Adv. Mater. (Weinheim, Ger.) **17**, 1673 (2005).
[37] S. E. Moulton, M. Maugey, P. Poulin, and G. G. Wallace, J. Am. Chem. Soc. **129**, 9452 (2007).
[38] M. F. Islam, A. M. Alsayed, Z. Dogic, J. Zhang, T. C. Lubensky, and A. G. Yodh, Phys. Rev. Lett. **92**, 088303 (2004).
[39] L. M. Ericson, H. Fan, H. Peng, V. A. Davis, W. Zhou, J. Sulpizio, Y. Wang, R. Booker, J. Vavro, C. Guthy, A. N. G. Parra-Vasquez, M. J. Kim, S. Ramesh, R. K. Saini, C. Kittrell, G. Lavin, H. Schmidt, W. W. Adams, W. E. Billups, M. Pasquali, W.-F. Hwang, R. H. Hauge, J. E. Fischer, and R. E. Smalley, Science **305**, 1447 (2004).
[40] N. Behabtu, M. Green, and M. Pasquali, Nanotoday **3**, 24 (2008).
[41] E. J. W. Verwey and J. T. G. Overbeek, *Theory of the Stability of Lyophobic Colloids* (Elsevier, Amsterdam, 1948).
[42] J. N. Israelachvili, *Intermolecular and Surface Forces* (Academic, London, 1992).
[43] D. Chapot, L. Bocquet, and E. Trizac, J. Chem. Phys. **120**, 3969 (2004).
[44] O. Pelletier, P. Davidson, C. Bourgaux, and J. Livage, Europhys. Lett. **48**, 53 (1999).
[45] H. Maeda and Y. Maeda, J. Chem. Phys. **121**, 12655 (2004).
[46] V. A. Davis, "Phase behavior and rheology of single-walled carbon nanotubes (SWNTs) in superacids with application to fiber spinning," Ph.D. thesis, Rice University, 2006.
[47] Y. Marcus, E. Pross, and N. Soffer, J. Phys. Chem. **84**, 1725 (1980).
[48] A similar effect is observed in DLVO theory for a fixed attractive force but a repulsive force that increases with increasing solvent quality.
[49] A number of factors will influence the relationship between the acid strength and the attractive potential, and these factors may vary from one SWCNT sample to another. The attractive potential is independent of SWCNT length and polydispersity, but experiments indicate that the solubility of a HiPco SWCNT sample in a given acid varies with diameter distribution, the frequency of defects in the SWCNT sidewalls, and the chemical effects of the oxidation and purification process on the SWCNT sidewalls.
[50] S. J. Zhang, I. A. Kinloch, and A. H. Windle, Nano Lett. **6**, 568 (2006).
[51] S. Varga, D. C. Williamson, and I. Szalai, Mol. Phys. **96**, 1695 (1999).
[52] A. N. G. Parra-Vasquez, I. Stepanek, V. A. Davis, V. C. Moore, E. H. Haroz, J. Shaver, R. H. Hauge, R. E. Smalley, and M. Pasquali, Macromolecules **40**, 4043 (2007).
[53] This may be accomplished by a numerical of experimental techniques. These include washing the initial SWCNT sample with a weaker acid, such as 98% sulfuric acid, to eliminate the shortest SWCNTs. also, fractionating a sample in the biphasic regime in a weaker superacid, such as 102% sulfuric acid, removing the isotropic phase can be used to eliminate the shortest SWCNTs.
[54] L. Li, M. Marjanska, G. H. J. Park, A. Pines, and A. P. Alivisatos, J. Chem. Phys. **120**, 1149 (2004).
[55] W. Song and A. H. Windle, Macromolecules **38**, 6181 (2005).
[56] W. Song, I. A. Kinloch, and A. H. Windle, Science **302**, 1363 (2003).